

See discussions, stats, and author profiles for this publication at: <https://www.researchgate.net/publication/51032965>

Bioconjugation of Luminescent Silicon Quantum Dots for Selective Uptake by Cancer Cells

ARTICLE *in* BIOCONJUGATE CHEMISTRY · JUNE 2011

Impact Factor: 4.51 · DOI: 10.1021/bc100552p · Source: PubMed

CITATIONS

50

READS

165

9 AUTHORS, INCLUDING:



[Wing-Cheung Law](#)

University at Buffalo, The State University of ...

79 PUBLICATIONS 2,416 CITATIONS

[SEE PROFILE](#)



[Hong Ding](#)

Florida International University

70 PUBLICATIONS 2,197 CITATIONS

[SEE PROFILE](#)



[Mark Swihart](#)

University at Buffalo, The State University of ...

212 PUBLICATIONS 6,016 CITATIONS

[SEE PROFILE](#)

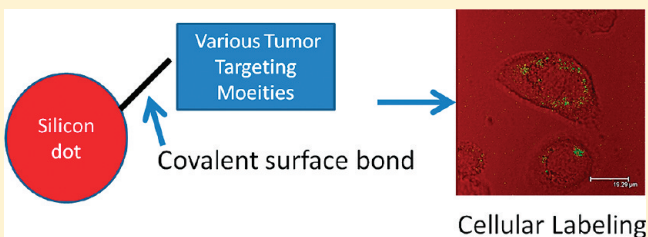
Bioconjugation of Luminescent Silicon Quantum Dots for Selective Uptake by Cancer Cells

Folarin Erogbogbo,^{†,§} Chen-An, Tien,[†] Ching-Wen Chang,[†] Ken-Tye Yong,[§] Wing-Cheung Law,[§] Hong Ding,[§] Indrajit Roy,[†] Mark T. Swihart,^{†,‡,*} and Paras N. Prasad^{†,§,*}

[†]Department of Chemical and Biological Engineering, [‡]Department of Chemistry and [§]Institute for Lasers, Photonics and Biophotonics, The University at Buffalo, State University of New York Buffalo, New York 14260-4200, United States

 Supporting Information

ABSTRACT: Conventional quantum dots have great potential in cancer-related imaging and diagnostic applications; however, these applications are limited by concerns about the inherent toxicity of their core materials (e.g., cadmium, lead). Virtually all imaging applications require conjugation of the imaging agent to a biologically active molecule to achieve selective uptake or binding. Here, we report a study of biocompatible silicon quantum dots covalently attached to biomolecules including lysine, folate, antimesothelin, and transferrin. The particles possess desirable physical properties, surface chemistry, and optical properties. Folate- and antimesothelin-conjugated silicon quantum dots show selective uptake into Panc-1 cells. This study contributes to the preclinical evaluation of silicon quantum dots and further demonstrates their potential as an imaging agent for cancer applications.



INTRODUCTION

Quantum dots (QDs) are semiconductor nanocrystals, 1–10 nm in diameter, that typically consist of combinations of elements from groups II and VI (CdSe, CdTe, CdS, ZnS, and ZnSe), groups IV and VI (PbS and PbSe), or groups III and V (GaAs, GaN, InP, and InAs) of the periodic table.^{1,2} They are attractive for optical imaging because of their size-tunable luminescence, high photostability, brightness, and broad excitation spectra that allow QDs with multiple emission wavelengths to be excited with a single source.^{3–5} By adopting techniques from drug delivery and targeted imaging technologies, heavy metal based quantum dots have been rapidly developed and investigated for many biological applications including optical imaging,⁶ sentinel lymph node mapping,⁷ and multiplex imaging.⁸ However, translation of these well-studied quantum dots to the clinic is inhibited by toxicity concerns that stem from their incorporation of toxic heavy metals such as cadmium.^{9–12} This has led to encapsulations strategies that create complex nanostructures with different toxicity profiles.¹³

Even though extensive studies have been performed to monitor the safety of II–VI quantum dots, completely overcoming the toxicity concerns is not yet possible.^{14–17} Thus, a re-evaluation of the fundamental materials at the core of the quantum dots is warranted. Silicon (Si) QDs may provide a breakthrough for quantum dot technology because they are based on a nontoxic element that is essential for human health, and the product of their degradation, silicic acid, can be readily excreted via the urine.^{4,18,19} Even though Si QDs are attractive from a toxicity perspective, key challenges must be overcome to ensure that Si QDs can match the promise of better-studied

quantum dots for biological applications. In particular, high quantum yield (QY) and long-term stability in water and biological media are essential.

The surface chemistry of Si QDs is of great interest, not only because this chemistry is much different from that of heavy metal based semiconductor nanostructures, but also because the Si QD's optical properties, which are the basis of their utility in bioimaging, strongly depend on the surface state of the particles. There have been a few reports on the synthesis and surface modification of Si QDs to improve their competitiveness with traditional quantum dots. Kortshagen's group has produced surface-modified Si QDs with QY above 70% at near-infrared wavelengths, for particles dispersed in organic solvents.²⁰ However, such high QY has not been achieved at shorter wavelengths or for Si QDs in aqueous dispersions. Sailor's group recently developed biodegradable porous silicon for imaging tumors via the enhanced permeation and retention (EPR) effect²¹ and showed that clearance of the material was satisfactory. The free-standing Si QDs used here and Sailor's porous silicon particles are expected to have similar degradation routes and low toxicity from the core material. However, there are substantial differences in the chemistry, structure, and luminescence properties, to the extent that Si QDs may be considered a different nanostructure from porous silicon. To demonstrate the potential for multiphoton excitation of Si QDs, He et al. measured emission of Si QDs upon two and three photon excitation QDs,²² while Kauzlauch

Received: December 7, 2010

Revised: March 28, 2011

Published: April 07, 2011

recently demonstrated two photon cellular imaging in macrophages.²³ Though promising, the luminescence from the Si QDs used for two photon cellular imaging was limited to the blue range of the spectrum. Tilley et al. showed nonspecific uptake of allylamine terminated blue-emitting Si QDs in HeLa cells.²⁴ Reipa's group²⁵ conjugated red emitting silicon nanoparticles to streptavidin, and demonstrated specific binding of the nanoparticles to biotinylated polystyrene beads. However, after bioconjugation, the particles emitted blue luminescence. Development of bioconjugation chemistry that maintains the size-tunable luminescence of Si QDs thus remains an important need for biological applications such as targeted imaging, where emission that does not compete with autofluorescence is desired. We previously fabricated micelle-encapsulated Si QDs with size-tunable emission wavelength for targeted imaging of cancer cells. This method takes advantage of the interaction between hydrophobic groups that allow Si QDs to be encapsulated into the hydrophobic core of the micelle. These were first demonstrated for *in vitro* imaging⁴ and more recently for *in vivo* targeted tumor imaging in small animals.²⁶ However, those micelle-encapsulated constructs, in which each micelle typically contains many Si QDs, are not ideal for all purposes. Thus, bioconjugation of individual Si QDs remains of great interest, especially through the direct conjugation to surface carboxyl groups.²⁷

Conventional QDs can be modified for targeting purposes via bioconjugation techniques that render them useful for multiple imaging applications. *In vivo*, long circulation times and clearance mechanisms that raise toxicity concerns may be overcome by using smaller particles that have short circulation times and can be excreted rapidly through the kidneys.²⁸ Though this is encouraging, it poses a different challenge because receptors for some biomolecules (such as folate) are present on renal cells.²⁹ Folate receptors (FR) are overexpressed on many types of cancer cells compared to normal cells, and they have some advantages compared to monoclonal antibodies, such as prolonged circulation times, low cost, and tumor to nontarget tissue ratios. FR's are also overexpressed in the kidneys. If heavy metal based quantum dots are used with folate-based targeting, toxicity concerns in the kidney would be increased just as they are for cancer therapeutic folate-toxin conjugates that undergo renal clearance. Even though there are no prior reports of Si-folate conjugates, renal toxicity from Si-folate conjugates is not an anticipated issue because no toxic components are included in the formulation. We recently observed low toxicity of folate-conjugated micelle-encapsulated silicon nanoparticle formations in MTS cytotoxicity assays.⁴

Here, we report the development of Si QD probes directly bound to biomolecules, including folate and antimesothelin, for targeted cancer cell imaging. As synthesized, carboxyl terminated Si QDs provide (i) stable luminescence; (ii) modifiable surface characteristics; and (iii) the potential to interface with biologically relevant molecules for an array of applications such as targeted cellular imaging. Undecylenic acid was the carboxylic acid of choice because of its demonstrated low toxicity (5000 mg/kg in mice), and it is one of the most effective ways of preventing the influences of oxidation of the silicon core.²⁷ Biologically relevant molecules conjugated via carbodiimide chemistry to the carboxylic acid group of the undecylenic acid included amino acids, vitamins, enzymes, proteins, and antibodies. Because folate has been demonstrated to be effective for targeting cancers in humans, folate terminated Si QDs were evaluated as

imaging agents. A schematic of the conjugation process is shown in Figure 1.

EXPERIMENTAL METHODS

Materials. Silane (SiH_4 , Voltaix, electronic grade, 99.999%), hydrofluoric acid (HF, Acros Organic, 48–51%), nitric acid (HNO_3 , EMD, 68–70%), undecylenic acid (Acros Organic, 99%), lysine (Sigma-Aldrich, 95%), 1-ethyl-3-(3-dimethylaminopropyl)carbodiimide (EDC, Pierce Biotechnology, 98–100%), dimethyl sulfoxide (DMSO, Fisher Scientific, 99.9%), folic acid (Sigma-Aldrich, >98%), antimesothelin (clone 5B2, dilution 1:20; Novocastra, Newcastle Upon Tyne, United Kingdom), apo-transferrin (Sigma-Aldrich, ≥97%), and *N*-hydroxysulfo-succinimide (Sulfo-NHS, Fluka, ≥98.5%) were all used as received if not otherwise noted. The silicon nanoparticles were prepared by decomposing silane (SiH_4) via high-temperature CO_2 laser pyrolysis in an aerosol reactor based on the method developed by Li et al.^{30,31} The raw product was a dark brown powder that was not photoluminescent. This product was collected without exposure to air and handled in a glovebox to prevent oxidation. The typical primary particle diameter in the aggregated raw silicon powder was approximately 10 nm.

Etching Procedure. To produce hydrogen-terminated photoluminescent Si QDs, the raw particles were dispersed in methanol, then etched in a mixture of hydrofluoric acid (48 wt %) and nitric acid (69 wt %) (10/1, v/v) for 2 to 4 min. Typically, 300 mg of silicon nanoparticles were dispersed in 30 mL of methanol by sonication. The silicon–methanol mixture was added to the acid mixture and stirred until the luminescence emission spectrum approached the desired color. At that point, 400 mL of methanol was added to quench the reaction. After washing the etched particles with a water–methanol mixture (3/1, v/v) three times (500 mL, 500 mL, 250 mL) to remove the adsorbed acid, we collected the particles on a poly(vinylidene fluoride) (PVDF) membrane filter (Millipore, hydrophilic Durapore, 0.1 μm pore size). Finally, the membrane was rinsed with pure methanol. The particles were finally sonicated from the membrane into vials containing undecylenic acid. All these steps were completed in the glovebox to prevent the oxidation of the Si QDs, which can reduce their photoluminescence quantum yield. The size of the particles after etching ranges from 5 nm down to 1 nm depending on the desired emission wavelength.

Si QD Functionalization. The hydrogen-terminated silicon QDs were dispersed in 20 mL of undecylenic acid to give a cloudy suspension. The reactant and the silicon particles were then transferred to a three-necked flask, and 20 mL of ethanol was added. Three freeze–pump–thaw cycles were used to remove dissolved oxygen from the mixture before reaction. The flask was then heated to 78.9 °C for 3 h, with stirring, under an argon atmosphere. The double bond on undecylenic acid reacts with the hydrogen-terminated silicon surface by hydrosilylation to give a covalent Si–C linkage on the surface of the Si QDs (Figure 1a). These surface-modified QDs can be dispersed in most nonpolar solvents such as chloroform, hexane, and toluene. After the reaction, the initially cloudy silicon dispersion became optically clear, confirming that reaction had occurred and the modified particles were dispersible in ethanol. To remove excess undecylenic acid, the silicon QDs were dialyzed against 3 L of ethanol three times with solvent change points of 30 min, 3 h, and 24 h in bags with MW cutoff of 7000. The purity of particles was verified by rotary evaporation, which produces a film

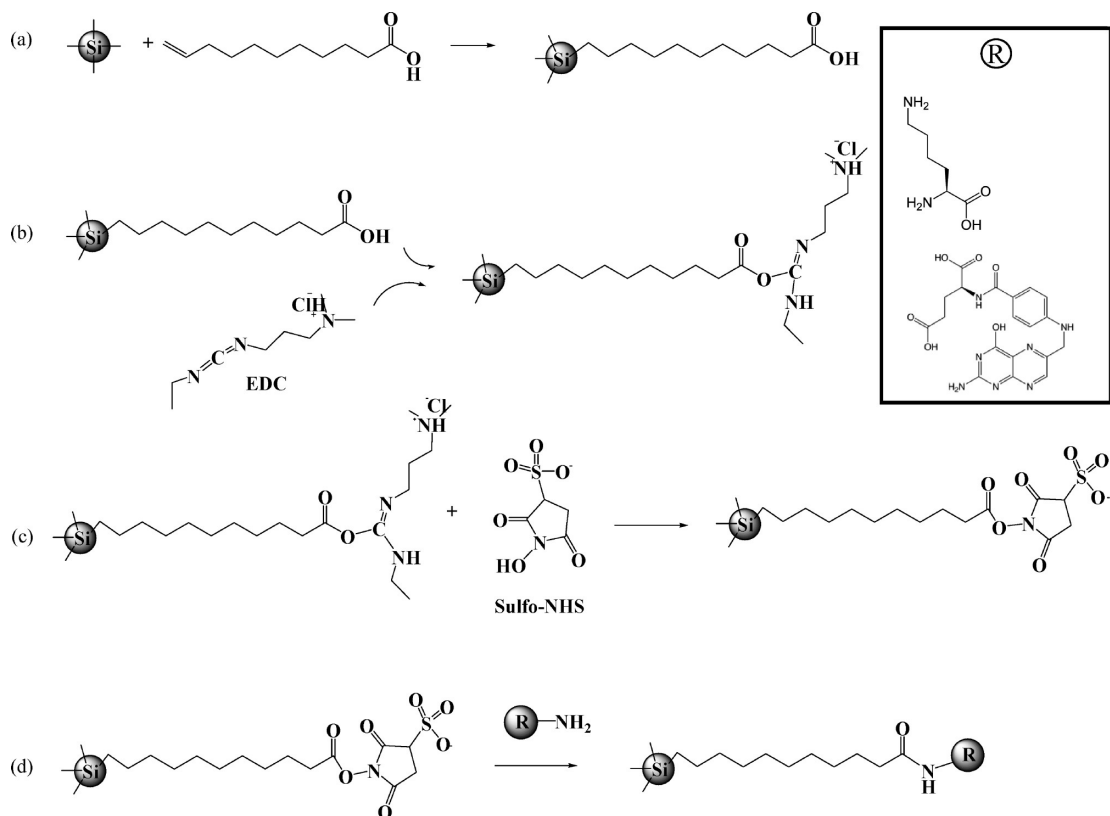


Figure 1. Schematic of surface functionalization and bioconjugation of silicon quantum dots: (a) hydrosilylation with undecylenic acid; (b) EDC coupling to form the o-acylisourea ester; (c) semistable amine reactive NHS-ester formation; (d) bioconjugation.

of undecylenic acid terminated Si QDs that can be readily dispersed in a variety of solvents and termination can be verified by FTIR.

Bioconjugation. In separate experiments, the Si QDs were conjugated to lysine, folic acid, antimesothelin, or apo-transferrin. An EDC-coupling reaction was used to form an amide bond between the carboxyl group on the Si QDs and a primary amine group on these reactants (Figure 1). Because the intermediate product of the EDC coupling was an unstable reactive o-acylisourea ester which could easily react with H₂O to regenerate the carboxyl group, we reacted sulfo-NHS with the o-acylisourea ester to produce a semistable amine-reactive NHS-ester. This amine-reactive NHS-ester consistently reacted with primary amines to yield a stable amide bond to the Si QDs. This implies that, ideally, we could conjugate any compound that has a primary amine group with Si QDs. To conjugate the Si QDs to folic acid, lysine, or transferrin, we started from 5 mL of the Si QD/ethanol sample and removed the ethanol by rotary evaporation. We next dissolved the Si QDs in 1 mL of DMSO. Eight milligrams of EDC and 8 mg of sulfo-NHS were each dissolved in 1 mL of LAL reagent water (LRW) or HPLC water, separately. These two compounds are unstable in water and must be freshly prepared for each experiment. The desired functional compound was also prepared in water (lysine or transferrin) or DMSO (folic acid) at 2 mg/mL. To start the EDC coupling reaction, 40 μ L of EDC–water solution was added into the vial containing the Si QDs. After stirring for 1 min, 40 μ L of sulfo-NHS was added, and stirring continued for 1 h to generate the semistable amine reactive NHS-ester. After forming the semistable intermediate, we separated the luminescent particles from the DMSO, EDC, and sulfo-NHS mixture by centrifugation. The particles then

were introduced into the lysine or transferrin aqueous solution (0.8 mL containing 1.6 mg biomolecule) or folic acid DMSO solution (60 μ L containing 0.12 mg folic acid). Initially, the mixture was cloudy, but after 15 min, the particles became well-dispersed. This reaction was carried out at room temperature for 1 h. Reaction products were separated by centrifugation at 10 000 g for 15 min after adding 1 mL of methanol to adjust the polarity of the solution to reduce the Si QD's dispersibility. The particles were washed by dispersing them in water, then collecting them by centrifugation thrice. For comparison, experiments were also performed using a one-step bioconjugation protocol, in which Si QDs were not separated from excess EDC and sulfo-NHS before adding the biomolecule to be conjugated to the particles. In the one-step protocol, the biomolecule was added to the reaction mixture \sim 5 min after adding the sulfo-NHS. The one-step method is more convenient and leads to fewer particle losses, but can also lead to cross-linking of biomolecules that have both amine and carboxyl functional groups, as discussed further below.

Cellular Imaging. Human pancreatic cancer cells (Panc-1) maintained in DMEM medium, with 10% fetal bovine serum (FBS) and appropriate antibiotic, were used for cellular imaging studies. As a standard, 8×10^5 cells are seeded for 100% confluence. One day before the treatment, an appropriate number of cells for 70–80% confluence were seeded in 35 mm cell culture dishes. On the day of treatment, the cells were incubated with bioconjugated Si QDs for 2 h at 37 °C at a confluence of 70–80%. After 2 h, cells were washed thrice with PBS, then imaged using a Leica laser scanning confocal microscope. The excitation wavelength used was 405 nm which was the shortest available wavelength on the microscope.

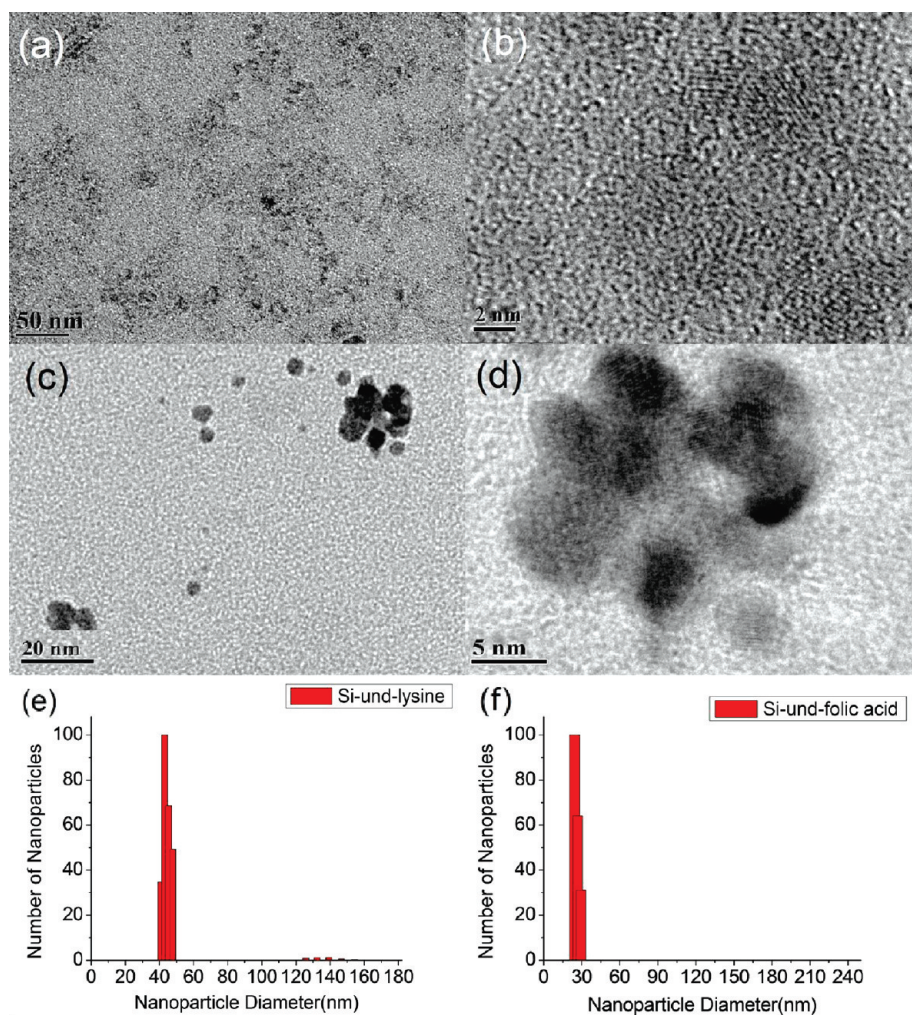


Figure 2. TEM images of (a,b) undecylenic acid terminated Si QDs and (c,d) Si QDs after bioconjugation to lysine. Hydrodynamic diameter distributions measured by DLS for (e) lysine-conjugated and (f) folic acid conjugated Si QDs. The mean diameter of Si-and-lysine particles is 46.7 nm, and the size of Si-and-folic acid particles is 26 nm.

Si QD Characterization. The silicon nanoparticles were characterized by transmission electron microscopy (TEM, JEOL 2010) before and after bioconjugation. Photoluminescence spectra (fluorescence spectra) were recorded with a Perkin-Elmer LS 50 fluorescence spectrometer with a 351 nm band-pass filter used to suppress any scattered light from the source. The excitation wavelength was set to 350 nm and the emission cutoff filter was set to 390 nm. Fluorescence quantum yield s (QYs) of the QD dispersions were determined by comparing the integrated emission from the QDs to rhodamine 6G dye solutions of matched absorbance. FTIR spectra were measured on a Bruker Vertex 70 spectrometer in attenuated total reflectance mode. The hydrodynamic diameter was measured by dynamic light scattering (BIC, 90 Plus). The uptake of bioconjugated Si QDs into pancreatic cancer cells was confirmed by laser confocal imaging (Leica Microsystems Semiconductor GmbH, Wetzlerm Germany, laser excitation at 405 nm).

RESULTS AND DISCUSSION

The size of the silicon nanoconstructs is shown in Figure 2. Figure 2a,b shows TEM images of the undecylenic acid-coated Si QDs at low and high magnification, respectively. Particles around

4–5 nm with lattice fringes are observed in Figure 2b. The average hydrodynamic diameter from DLS measurements was 23 nm. The large hydrodynamic diameter, relative to the crystalline core diameter, is attributed to the organic ligand on the surface of the silicon nanocrystals. These particles were conjugated with lysine using EDC and sulfo-NHS as depicted in Figure 1. After bioconjugation to lysine, some clusters are observed in the TEM images. The clusters are around 20 nm as seen in Figure 2d. The clusters consist of crystalline silicon QDs. Before the addition of lysine, the silicon content is estimated to be as high as 70% based on thermogravimetric analysis methods discussed previously,³² and the QY is $15 \pm 5\%$ before bioconjugation and $5 \pm 3\%$ after bioconjugation. The DLS-measured hydrodynamic diameter increased from 23 to 46 nm after bioconjugation with lysine. These sizes are from the two-step reaction. This increase in size is attributed to possible aggregation and cross-linking between lysine molecules. The lysine molecules possess carboxyl groups that form semistable NHS-ester groups and readily react with available amine groups of other lysine molecules. When the particles were conjugated in a one-step process, in which EDC, sulfo-NHS, and lysine were added sequentially without intermediate separation steps, the

size of the particles was around 100 nm in TEM images (Supporting Information Figure S1) and the DLS-measured mean hydrodynamic diameter was 150 nm. Even though it is much larger than the initial particle, the size of around 100 nm is

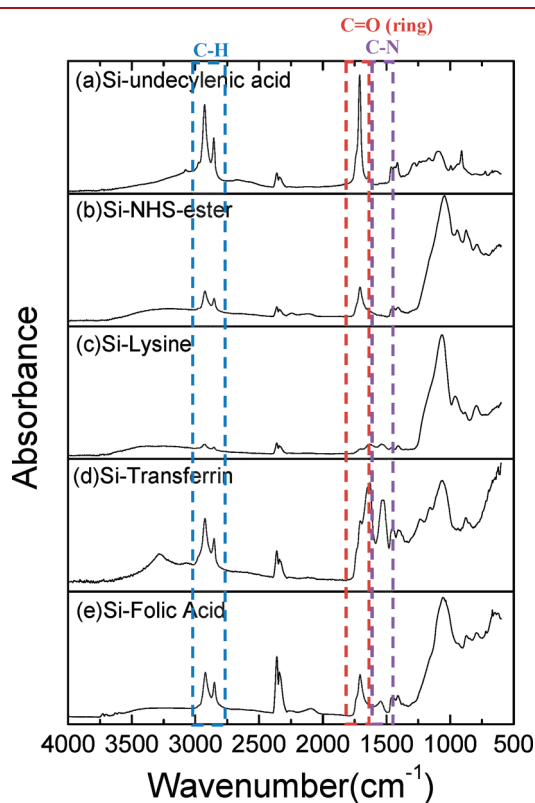


Figure 3. FTIR spectra of Si QDs after each step of the bioconjugation process.

favorable for some biological applications. To reduce cross-linking, a protocol that involved centrifugation between steps C and D in Figure 1 was used, as described above. This resulted in NHS-terminated Si QDs that were directly reacted with the amine groups of the lysine particles. The overall diameter of the particles was smaller in the two-step process because the excess lysine did not react with itself as much as in the one-step protocol. Similarly, the folate-conjugated particles had a hydrodynamic diameter of 26 nm using the two-step protocol and 120 nm using the one-step protocol. These data indicate that the carboxyl group on lysine has a higher tendency to cross-link to form larger particles or that these particles are less hydrophilic and have some tendency to aggregate in water.

Figure 3a displays the FTIR spectra of Si QDs after the hydrosilylation. The C–H stretch ($2929, 2855\text{ cm}^{-1}$), C–H bend ($1461, 1438, 1416\text{ cm}^{-1}$), and C=O stretch (1716 cm^{-1}) from the undecylenic acid are present in the spectrum. The absorbances at $3080, 2979, 2676$, and $913\text{--}947\text{ cm}^{-1}$ are assigned to the deformation bend and stretch vibrations of O–H (COOH) bond. Growth of the Si–C peak at 1240 cm^{-1} and the absence of the Si–H peaks near 2100 cm^{-1} indicate the full removal of Si–H bonds in the hydrosilylated nanoparticles³² (see Supporting Information Figure S2 for undecylenic acid FTIR spectrum). Figure 3b shows the FTIR spectrum of the semistable amine-reactive NHS-ester, in which the peak at 1707 cm^{-1} peak corresponds to the five-membered ring structure (see Supporting Information Figure S3 for the sulfo-NHS FTIR spectrum). Parts c, d, and e of Figure 3 show the IR spectra of the bioconjugated Si QDs. Figure 3d shows bands at 3270 cm^{-1} and 1635 cm^{-1} for amide A and amide I modes, respectively.³³ The amide III band is usually weak, but can be found at 1270 cm^{-1} . The absorbances at 1633 cm^{-1} and 1648 cm^{-1} in Figure 3d are assigned to α -helix and β -sheet structures. The peak at 1550 cm^{-1} is assigned to the C–N bond from the amide II group and the peak at 2252 cm^{-1} is from the

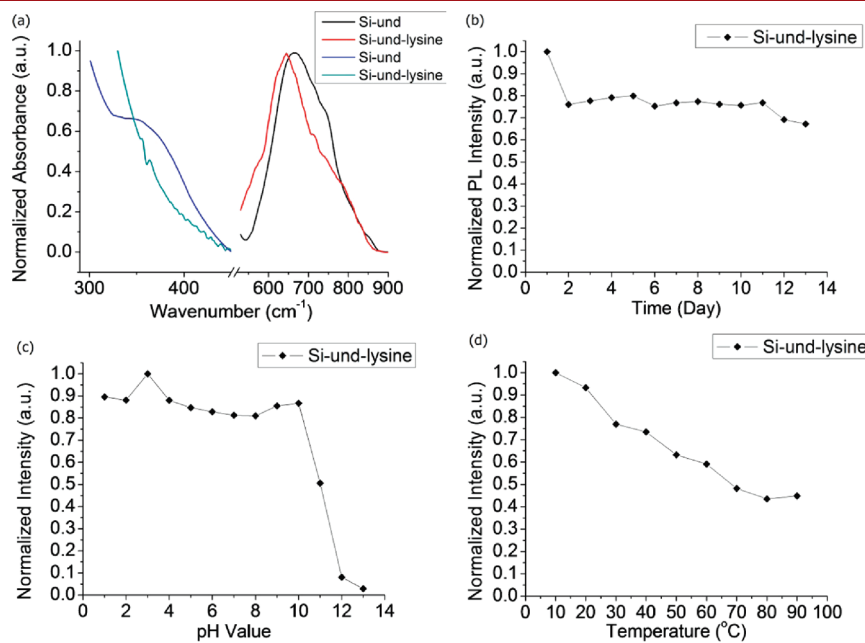


Figure 4. (a) Absorption and PL spectra undecylenic acid coated Si QDs (Si-und) and of lysine grafted Si QDs (Si-und-lysine) in a 50/50 (by volume) water/ethanol mixture. Stability of photoluminescence intensity from lysine grafted Si QDs in water, (b) over 13 days of storage at $4\text{ }^\circ\text{C}$, (c) at different pH levels in water, and (d) after heating to different temperatures in water. An average of three samples was used in the plots.

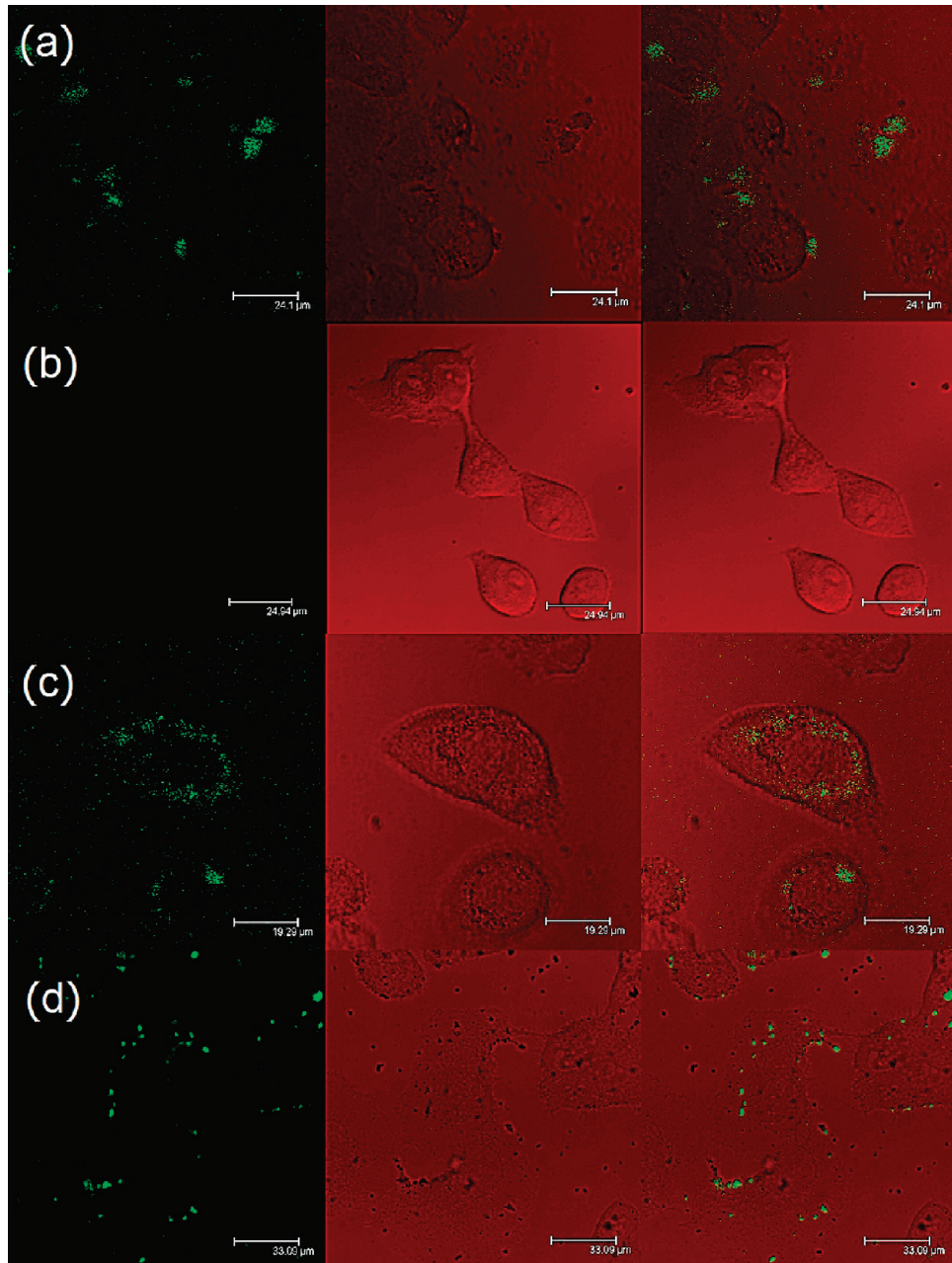


Figure 5. False-color confocal images of Panc-1 cells incubated with (a) lysine grafted Si QDs; (b) folic acid grafted Si QDs after incubation with excess folic acid; (c) folic acid grafted Si QDs; and (d) antimesothelin grafted Si QDs. From left to right, the panels show the luminescence images, the transmission images, and the overlay of the two. The scale bars are $24.1\text{ }\mu\text{m}$, $24.94\text{ }\mu\text{m}$, $19.29\text{ }\mu\text{m}$, and $33.09\text{ }\mu\text{m}$, respectively, in panels (a) through (d).

N–H bond on the silicon.³⁴ The six-membered ring structure has a very strong peak at 1710 cm^{-1} which confirmed the attachment of folic acid on Si QDs.

Figure 4a shows the absorption and PL emission spectra of undecylenic acid coated Si QDs and the PL of lysine-conjugated Si QDs. The emission peak shifts from 662 nm to 645 nm after the Si QDs are conjugated with lysine. Figure 4b shows the PL stability of the Si-lysine particles in water for 13 days. The first day after the bioconjugation, the Si QDs have the strongest photo luminescence intensity. Although the intensity dropped to 76% on the second day, the intensity remained stable for the next 11 days, until the 12th day when it dropped to 69%. This indicates that the undecylenic acid was reasonably effective in

protecting the Si QDs from oxidation. Even after the lysine conjugation and dispersion in water, the luminescence remained sufficiently stable for practical use over a period of at least two weeks. Figure 4c shows the PL intensity of lysine grafted Si QDs at different pH. From pH 1 to 10, it shows that Si QDs maintained a PL intensity that was at least 80% of the highest intensity at pH 3. Above pH 11, the PL intensity dropped drastically to 50.5% at pH 11, 8% at pH 12, and only 2% at pH 13. However, the PL is clearly stable over the entire range of biologically relevant conditions. Figure 4d displays the PL intensity of lysine-grafted Si QDs after heating to various temperatures. Although there is an obvious temperature dependence, the PL of the particles was higher than 40% of their initial

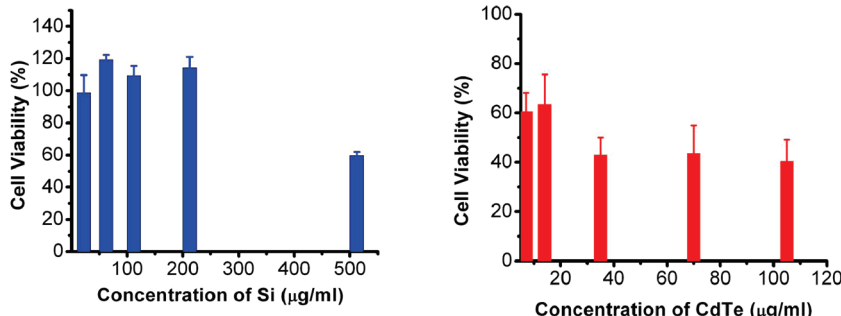


Figure 6. Cytotoxicity of (A) Si and (B) CdTe quantum dots toward Panc-1 cells. Error bars represent one standard deviation ($N = 3$). Note that the concentration range is much higher in (A) than in (B).

PL intensity at temperatures up to 90 °C. For in vivo application (30–40 °C), the PL intensity is more than 70% of the intensity at 10 °C.

To utilize Si QDs as an efficient targeted contrast agent for in vitro or in vivo imaging, the Si QDs must be conjugated with specific biorecognition molecules. Here, we present the conjugation of Si QDs with folate, antimesothelin, and transferrin. Panc-1 cells are an appropriate model to test cancer specific targeting by folate, transferrin, and antimesothelin because panc-1 cells have receptors for all three biomolecules.^{35,36} Since folate, transferrin, and anti mesothelin receptors are minimally distributed in normal cells/tissues, they serve as excellent ligands for preferentially targeting cancerous cells and tissues in vitro and in vivo. The biomolecule-conjugated nanoprobes are transported into cells or localized on the membrane through the corresponding receptor. Figure 5 shows confocal microscopy images of panc-1 cells stained with the Si QD bioconjugates. Figure 5a shows the nonspecific targeting of lysine coated Si-QDs. As seen in the images, the Si bioconjugates are associated with the cells, but do not appear to have been internalized.

Figure 5b shows the cellular image obtained when Panc-1 cells were presaturated with excess folic acid for 2 h then incubated with folic acid-conjugated Si QDs (FA-Si QDs). There is no visible luminescence from the image indicating that FA-Si QDs are not taken up when the folate receptors are presaturated. Figure 5c shows the confocal image of Panc-1 cells incubated with FA-Si QDs for 2 h, without the folic acid pretreatment. The FA-Si QDs appear to be transported into cells through the corresponding receptor, demonstrating selective uptake via the folate receptors. Transferrin-grafted Si QDs also labeled the cancer cells, though less effectively than the FA-Si QDs (Supporting Information Figure S4). Figure 5d is shows Panc-1 cells incubated with antimesothelin grafted Si QDs (AM-Si QDs). The particles appear to be localized on the membrane of the cells indicating the efficacy of AM-Si QDs. The lack of any visible cell damage in all images is consistent with the expected biocompatibility of the Si QDs.

As cell morphology is not ideal for evaluating the toxicity of nanoparticle alone, MTS assays were used for comparative studies between toxicity profiles of hydrogen-terminated Si QDs with cysteine-capped CdTe QDs. The minimal encapsulation (cysteine is used in the CdTe QD synthesis) is intended to assess the inherent cytotoxicity of the core components. Figure 6 shows the in vitro cytotoxicity results for Si and CdTe QDs on a human pancreatic cancer (Panc-1) cell line at 24 h post-treatment. The inhibitory particle concentrations corresponding to 50% cell viability (IC_{50}) were ~40 μg/mL for CdTe compared to >500 μg/mL

for the Si QDs. This demonstrates a significantly better toxicity profile for Si QDs when compared to Cd-based QDs.

■ DISCUSSION

Si QDs are beginning to become accepted as a nontoxic alternative to toxic quantum dots. The chemistry however has to be properly defined, and bioconjugation is one of the most important areas that must be investigated for the practical applications of SiQDs. The bioconjugation of SiQD can be challenging because standard protocols that are used for conventional quantum dots are not directly applicable to the functionalization of SiQDs. Short chain carboxyl groups like butenoic acid (results not shown) can produce bright orange luminescent particles; however, upon conjugation to lysine, the particles' emission becomes blue. This blue shifting also occurred when octane-terminated silicon nanoparticles were conjugated to DNA as luminescent labels.³⁷ It is important to maintain optical properties for imaging applications. Oxidation is normally responsible for the blue shift, and the method presented here prevents that complete blue shift from occurring. There is a very slight blue shift after conjugation; however, the particles are relatively stable as depicted in Figure 4. The particles are useful for labeling cancer cells with different targeting agents, which is of importance because targeted diagnosis and therapies are gaining traction in biomedical research.

■ CONCLUSION

A bioconjugation protocol for preparing smaller water-dispersible Si QDs has been developed and presented. A variety of appropriate functional groups for bioconjugation can be linked to the Si QDs for biological labeling. Antimesothelin and folic acid conjugated Si QDs were successfully applied for fluorescence imaging of pancreatic cancer cells. The excellent stability of the Si QDs in water provides longer observation time scale for targeting tumor cells without observable in vitro toxicity. Thus, the bioconjugated Si QDs presented here complement the larger micelle-encapsulated Si QD nanostructures we have previously developed, broadening the range of potential applications of Si QDs in biological imaging and diagnostics. This suggests that the Si QDs can be viable candidates for use in long-term and real-time cellular labeling and imaging.

■ ASSOCIATED CONTENT

S Supporting Information. TEM images of the lysine-conjugated Si QDs prepared via the one-step protocol, FTIR

spectra of sulfo-NHS and undecylenic acid, and confocal images of transferrin-grafted Si QDs-targeted Panc-1 cells. This material is available free of charge via the Internet at <http://pubs.acs.org>.

AUTHOR INFORMATION

Corresponding Authors

*E-mail: pnprasad@buffalo.edu, swihart@buffalo.edu.

ACKNOWLEDGMENT

This study was supported by grants from the NCI RO1CA119397, and the John R. Oishei Foundation.

REFERENCES

- (1) Prasad, P. N. (2003) *Biophotonics*, Wiley-Interscience, Hoboken, NJ.
- (2) Prasad, P. N. (2004) *Nanophotonics*, Wiley-Interscience, Hoboken, NJ.
- (3) Michalet, X., Pinaud, F. F., Bentolila, L. A., Tsay, J. M., Doose, S., Li, J. J., Sundaresan, G., Wu, A. M., Gambhir, S. S., and Weiss, S. (2005) Quantum dots for live cells, *in vivo* imaging, and diagnostics. *Science* 307, 538–544.
- (4) Erogogbo, F., Yong, K.-T., Roy, I., Xu, G., Prasad, P. N., and Swihart, M. T. (2008) Biocompatible luminescent silicon quantum dots for imaging of cancer cells. *ACS Nano* 2, 873–878.
- (5) Alivisatos, A. P. (1996) Semiconductor clusters, nanocrystals, and quantum dots. *Science* 271, 933–937.
- (6) Qian, X., Peng, X.-H., Ansari, D. O., Yin-Goen, Q., Chen, G. Z., Shin, D. M., Yang, L., Young, A. N., Wang, M. D., and Nie, S. (2008) *In vivo* tumor targeting and spectroscopic detection with surface-enhanced Raman nanoparticle tags. *Nat. Biotechnol.* 26, 83–90.
- (7) Kim, S., Lim, Y. T., Soltesz, E. G., De Grand, A. M., Lee, J., Nakayama, A., Parker, J. A., Mihaljevic, T., Laurence, R. G., Dor, D. M., Cohn, L. H., Bawendi, M. G., and Frangioni, J. V. (2004) Near-infrared fluorescent type II quantum dots for sentinel lymph node mapping. *Nat. Biotechnol.* 22, 93–97.
- (8) Stroh, M., Zimmer, J. P., Duda, D. G., Levchenko, T. S., Cohen, K. S., Brown, E. B., Scadden, D. T., Torchilin, V. P., Bawendi, M. G., Fukumura, D., and Jain, R. K. (2005) Quantum dots spectrally distinguish multiple species within the tumor milieu *in vivo*. *Nat. Med.* 11, 678–682.
- (9) Hoshino, A., Fujioka, K., Oku, T., Suga, M., Sasaki, Y. F., Ohta, T., Yasuhara, M., Suzuki, K., and Yamamoto, K. (2004) Physicochemical properties and cellular toxicity of nanocrystal quantum dots depend on their surface modification. *Nano Lett.* 4, 2163–2169.
- (10) Derfus, A. M., Chan, W. C. W., and Bhatia, S. N. (2003) Probing the cytotoxicity of semiconductor quantum dots. *Nano Lett.* 4, 11–18.
- (11) Dubertret, B., Skourides, P., Norris, D. J., Noireaux, V., Brivanlou, A. H., and Libchaber, A. (2002) *In vivo* imaging of quantum dots encapsulated in phospholipid micelles. *Science* 298, 1759–1762.
- (12) Lovric, J., Cho, S. J., Winnik, F. M., and Maysinger, D. (2005) Unmodified cadmium telluride quantum dots induce reactive oxygen species formation leading to multiple organelle damage and cell death. *Chem. Biol.* 12, 1227–1234.
- (13) McNeil, S. E. (2009) Nanoparticle therapeutics: a personal perspective. *Wiley Interdisciplin. Rev.: Nanomed. Nanobiotechnol.* 1, 264–271.
- (14) Hauck, T. S., Anderson, R. E., Fischer, H. C., Newbigging, S., and Chan, W. C. W. (2010) *In vivo* quantum-dot toxicity assessment. *Small* 6, 138–144.
- (15) Fitzpatrick, J. A. J., Andreko, S. K., Ernst, L. A., Waggoner, A. S., Ballou, B., and Bruchez, M. P. (2009) Long-term persistence and spectral blue shifting of quantum dots *in vivo*. *Nano Lett.* 9, 2736–2741.
- (16) Pons, T., Pic, E., Lequeux, N., Cassette, E., Bezdetnaya, L., Guillemin, F. o., Marchal, F. d. r., and Dubertret, B. (2010) Cadmium-free CuInS₂/ZnS quantum dots for sentinel lymph node imaging with reduced toxicity. *ACS Nano* 4, 2531–2538.
- (17) Ron, H. (2006) A toxicologic review of quantum dots: toxicity depends on physicochemical and environmental factors. *Environ. Health Perspect.* 114, 165–172.
- (18) Yong, K.-T., Qian, J., Roy, I., Lee, H. H., Bergey, E. J., Trampesch, K. M., He, S., Swihart, M. T., Maitra, A., and Prasad, P. N. (2007) Quantum rod bioconjugates as targeted probes for confocal and two-photon fluorescence imaging of cancer cells. *Nano Lett.* 7, 761–765.
- (19) Fujioka, K., Hiruoka, M., Sato, K., Manabe, N., Miyasaka, R., Hanada, S., Hoshino, A., Tilley, R. D., Manome, Y., Hirakuri, K., and Yamamoto, K. (2008) Luminescent passive-oxidized silicon quantum dots as biological staining labels and their cytotoxicity effects at high concentration. *Nanotechnology* 19, 415102.
- (20) Mangolini, L., Jurbergs, D., Rogojina, E., and Kortshagen, U. (2006) High efficiency photoluminescence from silicon nanocrystals prepared by plasma synthesis and organic surface passivation. *Phys. Status Solidi C* 3, 3975–3978.
- (21) Park, J.-H., Gu, L., von Maltzahn, G., Ruoslahti, E., Bhatia, S. N., and Sailor, M. J. (2009) Biodegradable luminescent porous silicon nanoparticles for *in vivo* applications. *Nat. Mater.* 8, 331–336.
- (22) He, G. S., Zheng, Q., Yong, K.-T., Erogogbo, F., Swihart, M. T., and Prasad, P. N. (2008) Two- and three-photon absorption and frequency upconverted emission of silicon quantum dots. *Nano Lett.* 8, 2688–2692.
- (23) Tu, C., Ma, X., Pantazis, P., Kauzlarich, S. M., and Louie, A. Y. (2010) Paramagnetic, silicon quantum dots for magnetic resonance and two-photon imaging of macrophages. *J. Am. Chem. Soc.* 132, 2016–2023.
- (24) Warner, J. H., Hoshino, A., Yamamoto, K., and Tilley, R. D. (2005) Water-soluble photoluminescent silicon quantum dots. *Angew. Chem., Int. Ed.* 44, 4550–4554.
- (25) Choi, J., Wang, N. S., and Reipa, V. (2008) Conjugation of the photoluminescent silicon nanoparticles to streptavidin. *Bioconjugate Chem.* 19, 680–685.
- (26) Erogogbo, F., Yong, K.-T., Roy, I., Hu, R., Law, W.-C., Zhao, W., Ding, H., Wu, F., Kumar, R., Swihart, M. T., and Prasad, P. N. (2010) *In vivo* targeted cancer imaging, sentinel lymph node mapping and multi-channel imaging with biocompatible silicon nanocrystals. *ACS Nano* 5, 413–423.
- (27) Clark, R. J., Dang, M. K. M., and Veinot, J. G. C. (2010) Exploration of organic acid chain length on water-soluble silicon quantum dot surfaces. *Langmuir* 26, 15657–15664.
- (28) Soo Choi, H., Liu, W., Misra, P., Tanaka, E., Zimmer, J. P., Itty Ipe, B., Bawendi, M. G., and Frangioni, J. V. (2007) Renal clearance of quantum dots. *Nat. Biotechnol.* 25, 1165–1170.
- (29) Leamon, C. P., and Low, P. S. (2001) Folate-mediated targeting: from diagnostics to drug and gene delivery. *Drug Discovery Today* 6, 44–51.
- (30) Li, X., He, Y., and Swihart, M. T. (2004) Surface functionalization of silicon nanoparticles produced by laser-driven pyrolysis of silane followed by HF–HNO₃ etching. *Langmuir* 20, 4720–4727.
- (31) Swihart, M. T. (2003) Vapor-phase synthesis of nanoparticles. *Curr. Opin. Colloid Interface Sci.* 8, 127–133.
- (32) Hua, F. J., Swihart, M. T., and Ruckenstein, E. (2005) Efficient surface grafting of luminescent silicon quantum dots by photoinitiated hydrosilylation. *Langmuir* 21, 6054–6062.
- (33) Rozenberg, M., and Shoham, G. (2007) FTIR spectra of solid poly-L-lysine in the stretching NH mode range. *Biophysical Chemistry* 125, 166–171.
- (34) Haris, P. I., and Severcan, F. (1999) FTIR spectroscopic characterization of protein structure in aqueous and non-aqueous media. *J. Mol. Catal. B* 7, 207–221.
- (35) Ryschich, E., Huszty, G., Knaebel, H. P., Hartel, M., Büchler, M. W., and Schmidt, J. (2004) Transferrin receptor is a marker of malignant phenotype in human pancreatic cancer and in neuroendocrine carcinoma of the pancreas. *Eur. J. Cancer* 40, 1418–1422.
- (36) Qian, J., Yong, K.-T., Roy, I., Ohulchanskyy, T. Y., Bergey, E. J., Lee, H. H., Trampesch, K. M., He, S., Maitra, A., and Prasad, P. N. (2007) Imaging pancreatic cancer using surface-functionalized quantum dots. *J. Phys. Chem. B* 111, 6969–6972.
- (37) Wang, L., Reipa, V., and Blasic, J. (2004) Silicon nanoparticles as a luminescent label to DNA. *Bioconjugate Chem.* 15, 409–412.